Journal of Materials Chemistry A

Accepted Manuscript

ROYAL SOCIETY OF CHEMISTRY

www.rsc.org/materialsA

Highly stable GeOx@C core-shell fibrous anodes for improved capacity in lithium-ion batteries

Meng Li,† Dan Zhou,† Wei-Li Song, Xiaogang Li and Li-Zhen Fan*

Key Laboratory of New Energy Materials and Technologies, Institute of Advanced Materials and Technology, University of Science and Technology Beijing, Beijing, 100083, China

† These two authors contribute equally to this work.

*Corresponding author: E-mail: fanlizhen@ustb.edu.cn; Tel./fax: +86-10-62334311

Abstract

As a promising high capacity electrode material for lithium-ion batteries, Germanium anode up to date is still restricted by the large volume change (>300%) during repeated cycling, which leads to short cycle life and poor cycle stability in practical application. To break through such barriers, herein a facile fabrication is reported to encapsulate GeO_x nanoparticles into hollow carbon shell using co-axial electrospinning. Such core-shell structure has shown remarkable improvements in alleviating the volume change of GeO_x during cycling, minimizing the contact area between electrolyte and GeO_x to form a stable solid electrolyte interface film, and providing enhanced electrical conductivity. In addition, Ge nanoparticles in the GeO_x composite can promote the reversible capacity for the reversible utilization of Li_2O. As a result, such GeO_x@C composite electrode exhibits excellent cycling ability with a reversible specific capacity of 875 mAh g^{-1} at 160 mA g^{-1} after 400 cycles, along with an improved rate capacity of 513 mAh g^{-1} at a high current density of 1600 mA g^{-1} upon 500 cycles.

Key words: Lithium ion batteries; Anode; Germanium Oxide; Core-shell structure; Co-axial electrospinning

1. Introduction

Nowadays, lithium-ion batteries have been widely used in various portable electronic devices, electric vehicles and hybrid electric vehicles because of their high energy and power densities.[1-3] To further meet the increasing requirement for high performance lithium-ion batteries, advanced anodes have been rapidly developed owing to their progressive advance of enhanced energy/power densities. Silicon (Si) (~4200 mAh g^{-1}) and germanium (Ge) (~1640 mAh g^{-1}) are regarded as highly promising anode materials for their high theoretical capacities.[4-9] Although Ge delivers lower capacity, it possesses much larger lithium-ion diffusion coefficient (400 fold higher) and electrical conductivity (10^4 fold higher) than that of Si.[10-12] Also, the high cost is expected to be reduced in the future because of its abundant natural resources,[13] and these unique features allow Ge to serve as an excellent candidate anode material for lithium-ion batteries.

Similar to Si, large volume change (>300%) of Ge during lithiation/delithiation process leads to stress-introduced cracking of the structures, and the pulverization results in poor cycling ability and capacity fading.[14-15] In addition, further capacity loss would happen due to the decreased lithium diffusion induced by the unstable solid electrolyte interface (SEI) film that is formed on the interface between Ge and the liquid electrolyte.[16] Various strategies have been recently carried out to address these unexpected bottlenecks, aiming to promote the energy storage performance of Ge-based anode materials. Exploratory efforts have been mainly focused on the design of Ge nanostructures with different morphologies and optimized size,[17-21] such as nanoparticles, nanowires, and nanotubes. Nevertheless, the bare anode materials usually suffer from low conductivity, aggregation, pulverization, etc. Another significant strategy is toward fabricating carbon-based hybrid composites that not only provide a buffer to restrict the expansion for lithium ion intercalation, but also form a

stable SEI layer for improving the electrical conductivity.[22-29]

Furthermore, the oxide form of Ge (GeO_x) has also been intensively studied lately due to its enhanced theoretical capacity up to 2152 mAh g^{-1} (storing 8.4 Li^+) (equation 1 and 2), while the irreversible Li_2O is often generated when GeO_2 undergoes a conversion reaction with Li, restricting the maximum capacity to 1126 mAh g^{-1} (storing 4.4 Li^+) (equation 2). In order to promote the kinetics of conversion reaction, an extra metal component like Cu and Ge has been incorporated into GeO_2 anodes.[30-33] The extra metal would play a catalytic role in the decomposition of Li_2O to facilitate the reoxidation of Ge. Thus, design of a functional nanoarchitecture that incorporates Ge with GeO_2 for GeO_x anodes should be an ideal approach to achieve the goal.

$$GeO_2 + 4Li \rightarrow Ge + 2Li_2O \quad (1)$$

$$Ge + 4.4Li \leftrightarrow Li_{4.4}Ge \quad (2)$$

For this purpose, encapsulation GeO_x nanoparticles into carbon matrices may be a promising design because the matrices can buffer the mechanical strain caused by the large volume expansion of the GeO_x nanoparticles during cycling. This structure could also allow Li_2O to be homogeneously dispersed inside the matrices and thus the contact between Ge and Li_2O could be improved, promoting the reversibility of conversion reaction as shown in equation 1. In this work, we design a GeO_x@C core-shell fibrous structure using the co-axial electrospinning[34-35]. The hollow carbon shell can not only act as an electrically conductive buffer layer to restrict the volume change of GeO_x during cycling, but also forms a stable SEI layer on the carbon shell. Furthermore, the phase separation of GeO_x into Ge and GeO_2 nanoparticles[27] during carbonization would increase the capacity of the electrode through improving the reversibility of conversion reaction. The advantageous features of the composite are demonstrated by the electrochemical performance of the

GeO_x@C composite electrode, which shows improved specific capacity, long cycle life and excellent stability as an anode material for lithium-ion batteries.

2. Experimental Section

2.1 Preparation of GeO_x nanoparticles

The precursor GeO_x was synthesized by a facile one-step reduction approach.[36] In a typical preparation, 1 g GeO_2 was firstly added in 15 mL deionized water, then adding 10 mL $NH_3 \cdot H_2O$ (28 %) into the above mixture. After being dispersed by magnetic stirring, a clear and transparent solution of GeO_3^{2-} ions was obtained. Then fresh aqueous $NaBH_4$ solution (1.8 g $NaBH_4$ dissolved in 20 mL deionized water at 0 °C) was added drop-wise into the above solution with magnetic stirring. After stirring for 12 h, a suspension containing brownish-red particles was obtained. The brownish-red precipitation was obtained by centrifugation for 3 times with each of deionized water and ethanol, and then was dried at 60 °C under vacuum for 8 h.

2.2 Preparation of GeO_x@C core-shell fibers

The GeO_x@C core-shell fibers were fabricated by the co-axial electrospinning process. In the typical preparation, the polymeric shell solution was prepared by dispersing polyacrylonitrile (PAN, 0.62 g) into N, N-dimethylformamide (DMF, 5 g) solution. On the other hand, the polymeric core solution was prepared by dissolving poly(methyl methacrylate) (PMMA, 0.52 g) and GeO_x (0.25 g) into the mixed DMF (2 g) and acetone solution (2 g). All of these two solutions were stirred at 40 °C for 6 h. Then the shell and core solutions were immediately loaded into plastic syringes that were equipped with the outer and inner channels of a dual nozzle. The flow rate of the shell and core solutions were all set at 0.025 mL min^{-1}. The high voltage applied to the dual nozzle was 9.00 kV, and the distance between the tip of the dual nozzle and the corrector was 10 cm. After

electrospinning, the electrospun fibers were peeled off from the corrector and then stabilization at 270 °C in air, followed by carbonization under nitrogen atmosphere at 700 °C for 3h (the heating rate all set at 5 °C min^{-1}). For comparison, the hollow carbon fibers were synthesized at the same conditions without the addition of GeO_x nanoparticles.

2.3 Materials characterizations

As-prepared GeO_x@C core-shell fibers were characterized by various techniques. X-ray diffraction (XRD) pattern was acquired on a Cu Kα radiation (Rigaku D/max-RB) at 40 kV and 30mA. X-ray photoelectron spectroscopy (XPS) measurement was determined on a K-alpha (Themo Fisher Scientific, ESCALAB 250xi). Thermogravimetric analysis was conducted on a TGA/DSC1 type instrument (Mettler Toledo, Switzerland) in air from 20-800 °C with a heating rate of 10 °C min^{-1}. The morphology of the samples was observed using a field-emission scanning electron microscopy (FE-SEM) performed on a ZEISS supra 55 system. In order to see the morphology of the electrode after 100 cycles, the electrolyte on it was removed by chemical etching with dimethyl carbonate (DMC).

The electrochemical characterizations were carried out by using two-electrode CR2032 coin cells. The electrodes were prepared by dispersing 85% active materials, 10% acetylene black (Super P) and 5% PVDF in N-methyl-2-pyrrolidene solution to form a homogeneous slurry. Then the slurry was uniformly spread on Cu foil current collector, followed by drying at 60 °C in a vacuum oven overnight. The CR2032 coin cells were assembled in an argon-filled glove box. The electrolyte was 1 M $LiPF_6$ in ethylene carbonate/dimethyl carbonate/ethylmethyl carbonate (1:1:1) and the counter electrode was lithium metal. The batteries were discharged and charged on the battery test system (LAND CT2001A，Wuhan Jinnuo) in the voltage range of 0.005-3.0 V *vs.* Li/Li^+ at 25 °C. The cyclic

voltammetry (CV) performance was measured in the potential range of 0.005-3.0 V at a scan rate of 0.2 mV s^{-1} using electrochemical workstation (CHI660c, Shanghai Chenhua). Electrochemical impedance spectroscopy (EIS) were measured from 100 kHz to 0.1 Hz with an AC amplitude of 5 mV using electrochemical workstation (CHI660c, Shanghai Chenhua). If not mentioned, all the reported capacities are based on the total mass of GeO_x@C composite.

3. Results and discussion

The GeO_x@C core-shell fibers were fabricated by the co-axial electrospinning process, as briefly illustrated in Fig. 1. The polymeric shell solution was prepared by dissolving PAN into the DMF solution, while the polymeric core solution was prepared by dissolving GeO_x nanoparticles and PMMA into a mixture solution. After co-axial electrospinning and carbonization, a core-shell structure that encapsulates GeO_x nanoparticles into hollow carbon fibers was obtained.

The core-shell structure of the fibers is confirmed by SEM. As exhibited in Fig. 2a, the average size of the bare GeO_x nanoparticles is about 100 nm. The resulting GeO_x@C core-shell fibers present a smooth feature with a uniform diameter of 1 um (Fig. 2b and 2c). In addition, the cross-sectional image of a single fiber (Fig. 2d) confirms that the GeO_x nanoparticles have been well encapsulated into the hollow carbon shell. Furthermore, enough internal void space has also been observed between the GeO_x nanoparticles and carbon shell, which is associated with the decomposition of PMMA during carbonization. The formation of the void spaces is necessary to alleviate the large volume expansion of GeO_x, preventing the GeO_x nanoparticles from pulverization during the repeated cycling.

The crystal structures of the pure GeO_x nanoparticles and GeO_x@C composite were characterized by XRD, as shown in Fig. 3a. The pure GeO_x nanoparticles were prepared by a facile

one-step reduction approach at room temperature. The broad peak observed at 2θ of 20-35° in pure GeO_x sample indicated the amorphous feature. After carbonization, the major diffraction peaks at 2θ=27.283, 45.305, 53.682, 66.015, 72.802 and 83. 685 could be assigned to be (111), (220), (311), (400), (331) and (422) planes, respectively, which suggests formation of the diamond cubic Ge (JCPDS no. 65-0333). The broad peak is presumably attributed to the amorphous structure of GeO_2 and carbon. The chemical compositions of the sample were further investigated by XPS. Fig. 3b demonstrates the typical element distribution of the composite and Fig. 3c shows that the Ge 2p spectrum involves two peaks. The main peak at 1217.20 eV is assigned to Ge-Ge, and the higher peak at 1220.60 eV is assigned to Ge-O-Ge. According to Fig. 3d, the existence of oxygen can be assigned to Ge-O-Ge and -$COOCH_3$. These confirm that the GeO_x in the GeO_x@C composite presented phase separation and crystalline Ge was formed after amorphous GeO_2 was carbonized.[27] Though GeO_2 nanoparticles would introduce irreversible Li_2O during cycling, the existence of Ge nanoparticles can promote the reversible utilization of Li_2O and the reoxidation of Ge. Therefore, the formation of GeO_x nanoparticles can enlarge the total capacity of the GeO_x@C composite. For quantifying the amount of GeO_x and amorphous carbon in the GeO_x@C composite, TGA was carried out in air and the content of GeO_x was calculated to be about 42% (Fig. S1).

Fig. 4a shows the charge/discharge voltage profiles of GeO_x@C composite at a current density of 160 mA g^{-1} in the voltages between 0.005 and 3.0 V. The initial discharge and charge specific capacities of the GeO_x@C composite electrode reach 1392 and 973 mAh g^{-1}, respectively, with an initial coulombic efficiency of 70 %. The initial capacity loss is due to the formation of SEI film on the surface of the hollow carbon fibers coupled with the irreversible Li insertion into the carbon matrix.[37-38] Compared to the bare GeO_x nanoparticles with a coulombic efficiency about 40% at first

cycle (Fig. S2), the GeO_x@C composite electrode demonstrates significant improvement. The enhanced coulombic efficiency may be attributed to the hollow carbon fibers, which minimized the contact area between electrolyte and GeO_x nanoparticles and also the Ge nanoparticles, which could facilitate the decomposition of Li_2O. Moreover, no pronounced plateau has been found in the charge/discharge curves of GeO_x@C core-shell composite electrode (Fig. 4a), which is due to the amorphous structure of GeO_2 in the GeO_x. As plotted in Fig. 4b, the reversible capacity changes from 979 (the 2nd cycle) to 875 mAh g^{-1} (the 400th cycle) at a rate of 160 mA g^{-1}, and almost 90 % of the second discharge capacity remained. Furthermore, the coulombic efficiency is stable above 99.5 % after 10 cycles (Fig. S3). The high coulombic efficiency indicated the importance of the encapsulation of GeO_x nanoparticles in the hollow carbon fibers for the formation of stable SEI layers. For the bare GeO_x nanoparticles, under the same conditions, the discharge capacity quickly decreases to 235 mAh g^{-1} after 100 cycles. The sharp capacity fading can be related to the pulverization of GeO_x, which makes GeO_x nanoparticles lose contact with the current collector.[30] Moreover, the capacity contribution of GeO_x nanoparticles in the composite was also calculated based on the weight of GeO_x. After 400 cycles, GeO_x nanoparticles delivered discharge capacity of 1786 mAh g^{-1}, which is higher than the theoretical capacity of Ge (1640 mAh g^{-1}), indicating the full utilization of Ge and GeO_2 nanoparticles. Cyclic voltammetry of GeO_x@C composite electrode was applied in the potential window from 0.005 to 3 V at a scan rate of 0.2 mV s^{-1}. Obviously, no pronounced redox peaks were observed, which is consistent with the results in Fig. 4a. In the first cathodic scan, the voltage region between 0.9 and 0.01 V could be related to the electrochemical conversion of GeO_x to Ge and Ge to $Li_{4.4}Ge$. In the corresponding anodic scan, the broad peak between 0.2 to 0.7 V could be related to the de-alloying of $Li_{4.4}Ge$, while the subsequent broad peak

at 1.1 V could be linked to the regeneration of GeO_2 from Ge and Li_2O.[30] The overlapped curves in the following CV scans, including the reoxidation of Ge at 1.1 V, indicate the reversibility of Li_2O in the composite due to the catalytic role of Ge. The rate capability performance of GeO_x@C composite electrode is shown in Fig. 4c, which exhibits discharge capacities of 965, 808, 728, 612, 498, 392, and 286 mAh g^{-1} at 0.08, 0.32, 0.8, 1.6, 3.2, 4.8, and 8 A/g, respectively. Even at high current density of 4.8 A g^{-1}, a favorable specific capacity could be also achieved, which is still higher than the capacity of commercial graphite electrode (372 mAh g^{-1}). The specific capacity of the electrode after 500 cycles at 1.6 A g^{-1} was able to stay at a high reversible values (513 mAh g^{-1}), which implies the long cycle life and good cycle stability of the GeO_x@C composite electrode.

In order to further investigate the enhanced electrical conductivity of the GeO_x@C core-shell fibers in comparison with that of the bare GeO_x nanoparticles, an electrochemical impedance spectroscopy was conducted. Fig. 4e depicts the comparison of the Nyquist plots for the GeO_x@C composite and the bare GeO_x electrodes in the fully charged state (3 V *vs*. Li/Li^+) after 20 cycles. All the electrodes involve one depressed semicircle in the high frequency region, along with a sloping straight line in the low frequency region. Generally, the diameter of the depressed semicircle is ascribed to the overlap between the resistance of SEI film and the Li^+ charge-transfer impedance on the electrode/electrolyte interface, while the sloping line corresponds to the lithium ion diffusion impedance.[39-40] Apparently, the GeO_x@C composite electrode shows a much lower diameter than the bare GeO_x electrode. This result indicates that GeO_x@C electrode possesses a high electrical conductivity due to a stable SEI film formed on the surface of the hollow carbon shell, which also offers fast charge-transfer channels. The EIS results also support that the structure of GeO_x@C composite could reduce the internal resistance of the electrode, resulting in better cycle and rate

performance in comparison with the bare GeO_x electrode.

To confirm the structure stability of this GeO_x@C core-shell fibrous electrode, a morphological study was conducted before cycles and after 100 cycles at a current density of 160 mA g^{-1}. SEM images on the surface of those electrodes are shown in Fig. 5. For the electrode after 100 cycles, the electrolyte was removed by chemical etching with dimethyl DMC. According to Fig. 5a and 5c, the two electrodes before and after cycling exhibit a similar smooth surface. Notably, the morphology of the fibers remains unchanged and no obvious pulverization was observed after 20 cycles (Fig. 5b and 5d). The observed rough surface may refer to the formation of SEI layer. This result indicates that the GeO_x@C core-shell structure can alleviate the volume change of GeO_x nanoparticles and form a stable SEI layer, thus leading to a long cycle life and good cycling stability.

As listed in Table S1, comparison of typical previous report suggests that the electrochemical performance of the GeO_x@C core-shell composite is highly competitive, which is attributed to the unique properties of the core-shell structure design. A schematic of the lithiation and delithiation of the bare GeO_x and GeO_x@C composite electrodes during repeated cycles is presented in Fig. 6. Firstly, the GeO_x nanoparticles can be encapsulated by the hollow carbon fibers, suppressing the fracture of the GeO_x nanoparticles during repeated volume change. Moreover, enough void between the GeO_x nanoparticles and carbon shell acts as buffer space for the expansion of the GeO_x nanoparticles. Additionally, the hollow carbon fibers can provide an enhanced electrical pathway for the electrochemical reaction between Li and GeO_x, improving the rate capability performance. Besides, the Ge nanoparticles in the GeO_x@C composite would play a catalytic role to promote the decomposition of Li_2O and the reoxidation of Ge.

4. Conclusion

In summary, a high-performance GeO_x@C core-shell composite electrode is fabricated by co-electrospinning. This unique structure can take advantage of the carbon shell, including alleviation of the volume change of GeO_x during repeated cycles, facilitation of forming a stable SEI layer and enlargement of fast electronic and ionic transfer channels. Furthermore, the presence of Ge in the GeO_x composite can increase the reversibility of conversion reaction of GeO_2. This GeO_x@C core-shell fibrous electrode can not only exhibit excellent lithium storage performance, with stable reversible capacity and excellent rate capability, but also provides a preferable approach to other electrode materials that undergo large volume change during cycling.

Acknowledgements

The authors gratefully acknowledge financial support from National Basic Research Program of China (973 program) (No. 2015CB932500, 2014CB643300 and 2013CB934001), NSF of China (51172024 and 51372022) and Ministry of Education (20130006110019).

References

1. J. B. Goodenough and Y. Kim, *Chem. Mater.*, 2010, **22,** 587.

2. L. Q. Mai, X. C. Tian, X. Xu, L. Chang and L. Xu, *Chem. Rev*., 2014, **114,** 118228.

3. B. Kang and G. Ceder, *Nature*, 2009, **485,** 190.

4. C. K. Chan, H. Peng, G. Liu, K. Mcllwarth, X. F. Zhang, R. A. Huggins and Y. Cui, *Nat. Nanotechnol*., 2008, **3,** 31.

5. N. Liu, H. Wu, M. T. McDowell, Y. Yao, C. Wang and Y. Cui, *Nano Lett.*, 2012, **12,** 3315.

6. Z. Lu, N. Liu, H.-W. Lee, J. Zhao, W. Y. Li, Y. Z. Li and Y. Cui, *ACS Nano,* 2015, **9,** 2540.

7. C. K. Chan, X. F. Zhang and Y. Cui, *Nano Lett.*, 2008, **8,** 307.

8. X. H. Liu, S. Huang, S. T. Picraux, J. Li, T. Zhu and J. Y. Huang, *Nano Lett.*, 2011, **11,** 3991.

9. K. H. Seng, M.-H. Park, Z. P. Guo, H. K. Liu and J. Cho, *Angew. Chem. Int. Ed.*, 2012, **51,** 5657.

10. D. W. Wang, Y. L. Wang, Q. Wang, J. Cao, D. B. Famer, R. G. Gordon and H. J. Dai, *J. Am. Chem. Soc*., 2004, **126,** 11602.

11. X. Su, Q. L. Wu, J. C. Li, X. C. Xiao, A. Lott, W. Q. Lu, B. W. Sheldon and J. Wu, *Adv. Energy Mater.*, 2014, **4,** 1300882.

12. X. H. Liu and J. Y. Huang, *Energy Environ. Sci*., 2011, **4,** 3844.

13. J. Graetz, C. C. Ahn, R. Yazami and B. Fultz, *J. Electrochem. Soc*., 2004, **151,** A698.

14. F.-W. Yuan, H.-J. Yang and H.-Y. Tuan, *ACS Nano*, 2012, **6,** 9932.

15. C. Zhong, J.-Z. Wang, X.-W. Gao, D. Wexler and H.-K. Liu, *J. Mater. Chem. A*, 2013, **1,** 10798.

16. H. Wu and Y. Cui, *Nano Today*, 2012, **7,** 414.

17. Y. Son, M. Park, Y. Son, J.-H. Jang, Y. Kim and J. Cho, *Nano Lett.*, 2014, **14,** 1005.

18. T. Kennedy, E. Mullane, H. Geaney, M. Osiak, C. O'Dwyer and K. M. Ryan, *Nano Lett*., 2014, **14,** 716.

19. M.-H. Park, Y. Cho, K. Kim, J. Kim, M. Liu and J. Cho, *Angew. Chem. Int. Ed*., 2011, **123,** 9821.

20. M.-H. Park, K. Kim, J. Kim and J. Cho, *Adv. Mater*., 2010, **22,** 415.

21. W. Li, Y.-X. Yin, S. Xin, W.-G. Song and Y.-G. Guo, *Energy Environ. Sci*., 2012, **5,** 8007.

22. D. Li, C. Feng, H. K. Liu and Z. P. Guo, *J. Mater. Chem. A*, 2015, **3,** 978.

23. M. Gu, Y. Li, X. Li, S. Hu, X. Zhang, W. Xu, S. Thevuthasan, D. R. Baer, J.-G. Zhang, J. Liu and C. Wang, *ACS Nano*, 2012, **6,** 8439.

24. W. H. Li, Z. Z. Yang, J. X. Cheng, X. W. Zhong, L. Gu and Y. Yu, *Nanoscale*, 2014, **6,** 4532.

25. J. Wang, J.-Z. Wang, Z.-Q. Sun, X.-W. Gao, C. Zhong, S.-L. Chou and H.-K. Liu, *J. Mater. Chem. A*, 2014, **2,** 4613.

26. F.-W. Yuan and H.-Y Tuan, *Chem. Mater.*, 2014, **26,** 2172.

27. D. Li, K. H. Seng, D. Q. Shi, Z. X. Chen, H. K. Liu and Z. P. Guo, *J. Mater. Chem. A*, 2013, **1,** 14115.

28. S. X. Jin, N. Li, H. Cui and C. X. Wang, *ACS Appl. Mater. Interfaces*, 2014, **6,** 19397.

29. J. Liu, K. Song, C. B. Zhu, C.-C. Chen, P. A. Aken, J. Maier and Y. Yu, *ACS Nano*, 2014, **8,** 7051.

30. K. H. Seng, M.-H. Park, Z. P. Guo, H. K. Liu and J. Cho, *Nano Lett*., 2013, **13,** 1230.

31. D. P. Lv, M. L. Gordin, R. Yi, T. Xu, J. X. Song, Y.-B. Jiang, D. Choi and D. H. Wang, *Adv. Funct. Mater*., 2014, **24,** 1059.

32. X.-L. Wang, W.-Q. Han, H. Y. Chen, J. M. Bai, T. A. Tyson, X.-Q. Yu, X.-J. Wang and X.-Q. Yang, *J. Am. Chem. Soc.*, 2011, **133,** 20692.

33. J. Hwang, C. Jo, M. G. Kim, J. Chun, E. Lim, S. Kim, S. Jeong and Y. Kim, *ACS nano,* 2015, **9,** 5299.

34. T. H. Hwang, Y. M. Lee, B.-S. Kong, J.-S. Seo and J. W. Choi, Nano Lett., 2012, **12,** 802.

35. L. Kou, T. Huang, B. Zheng, Y. Han, X. Zhao, K. Gopalsamy, H. Sun and C. Gao, Nat. Commun., 2014, **5,** 3754.

36. C. B. Jing, X. D. Zang, W. Bai, J. Bai, J. H. Chu and A. Y. Liu, *Nanotechnol*., 2010, **20,** 505607.

37. M. Wachtler, M. Winter and J. O. Besenhard, *J. Power Sources*, 2002, **105,** 151.

38. C. J. Zhang, Z. Lin, Z. Z. Yang, D. D. Xiao, P. Hu, H. X. Xu, Y. L. Duan, S. Pang, L. Gu and G. L. Cui, *Chem. Mater.*, 2015, **27,** 2189.

39. R. Ruffo, S. S. Hong, C. K. Chan, R. A. Hugggins and Y. Cui, *J. Phys. Chem. C*, 2009, **113,** 11390.

40. J. C. Guo, X. L. Chen and C. S. Wang, *J. Mater. Chem*., 2010, **20,** 5035.

Figure captions:

Figure 1. Schematic illustration of preparation the GeO_x@C core-shell fibers.

Figure 2. (a) SEM images of bare GeO_x nanoparticles; (b-c) SEM images of GeO_x@C core-shell fibers at low and high magnifications. (d) Cross-sectional SEM image of a single GeO_x@C core-shell fiber.

Figure 3. (a) XRD patterns of the bare GeO_x nanoparticles and GeO_x@C core-shell fibers. (b) The full XPS spectrum of GeO_x@C composite. (c) High-resolution Ge 2p XPS spectrum of GeO_x@C composite. (d) High-resolution XPS spectrum of the O 1s peak marked with a dash rectangle in (b).

Figure 4. Electrochemical performance for GeO_x@C compsoites: (a) charge-discharge potential profiles of GeO_x@C composite electrode at different cycles. The cell was measured at 160 mA g^{-1}; (b) the cycling performance of bare GeO_x, carbon and GeO_x@C electrodes at 160 mA g^{-1}; (c) rate capability of GeO_x@C composite electrode; (d) cyclic voltammetry investigation of GeO_x@C composite electrode at a scan rate of 0.02mV s^{-1} between 0.005~3V; (e) Nyquist plots of bare GeO_x and GeO_x@C composite electrodes in the fully charged state after 20 cycles, insert is the equivalent circuit used to model the impedance spectra.

Figure 5. SEM images of GeO_x@C composite electrode before cycling (a and b), and after 100 cycles (c and d).

Figure 6. Schematic of the lithium reaction mechanisms of bare GeO_x (a) and GeO_x@C (b) composite electrodes. The carbon shell in GeO_x@C composite electrode can not only act as buffer layer to suppress the fracture of the GeO_x nanoparticles during repeat cycles but also form stable SEI layer to provide an enhanced electrical pathway for the electrochemical reaction between Li and GeO_x.

Figures:

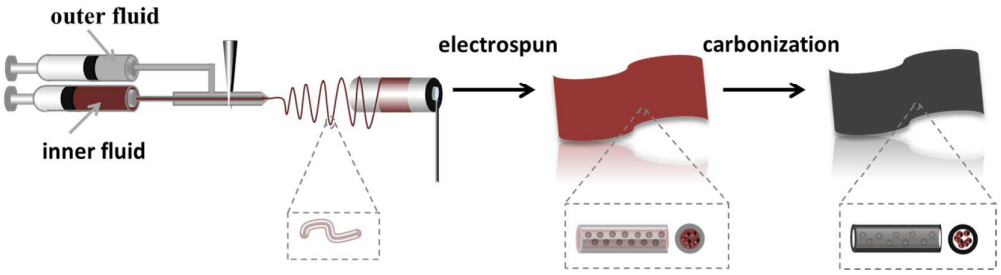

Figure 1

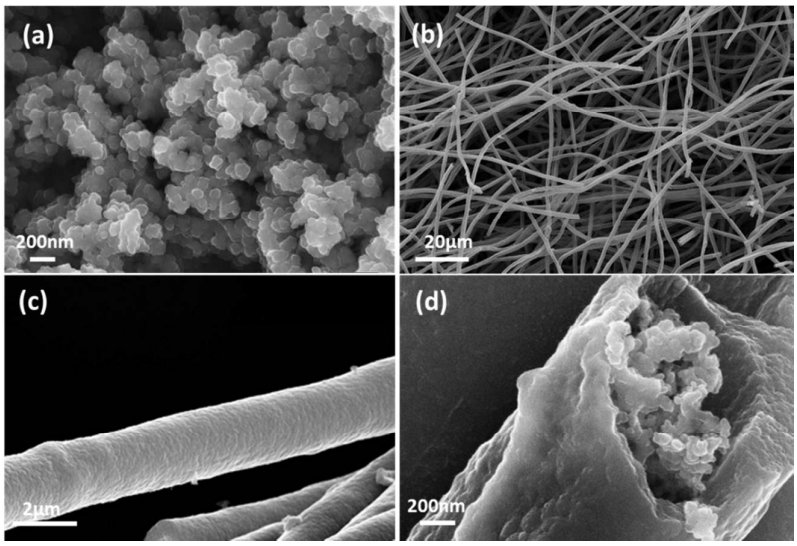

Figure 2

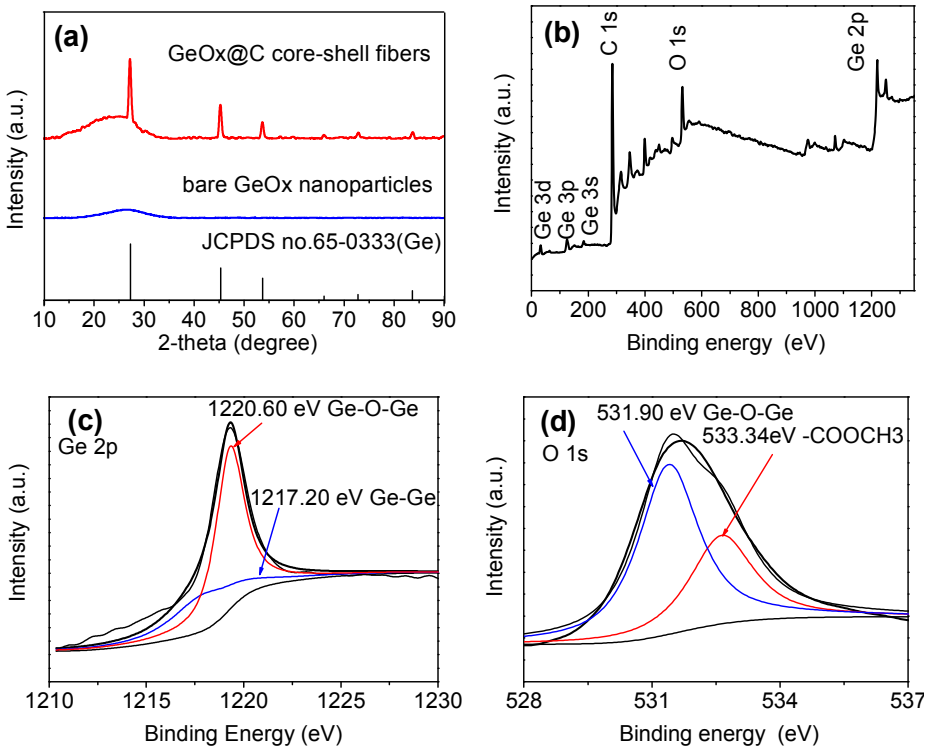

Figure 3

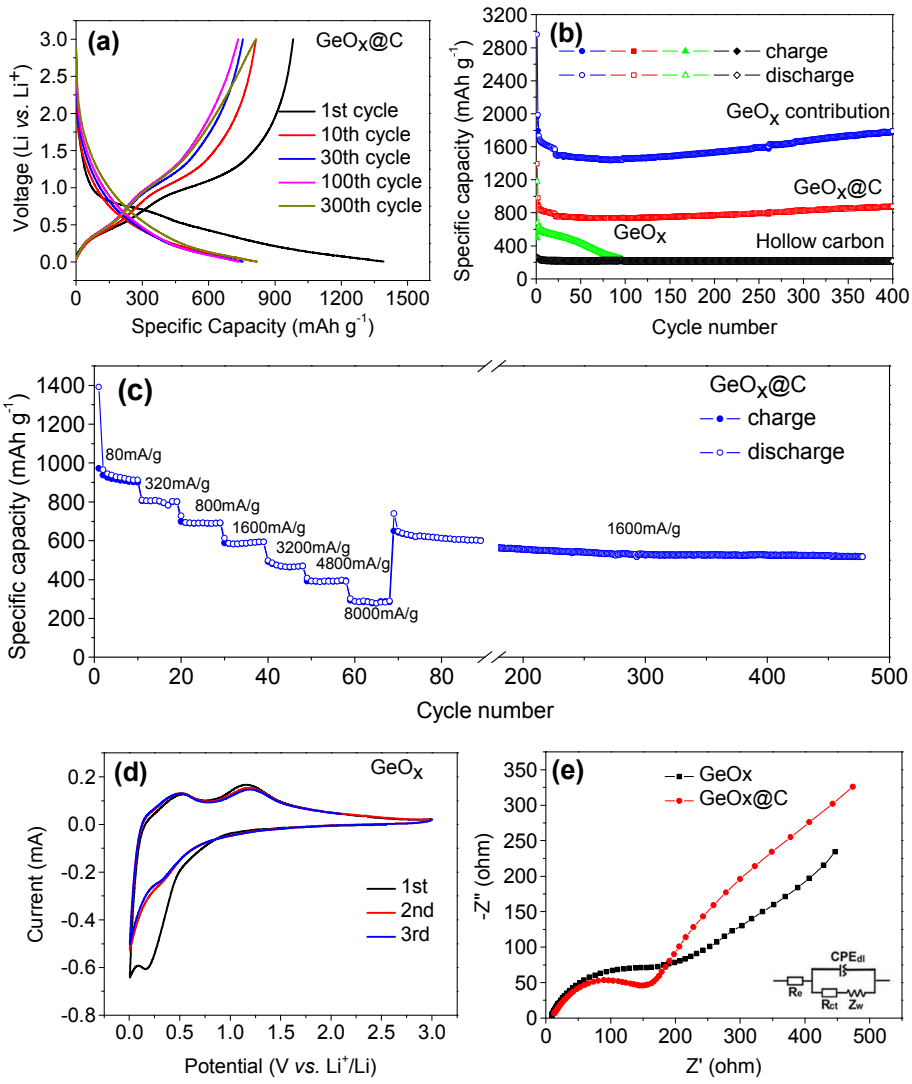

Figure 4

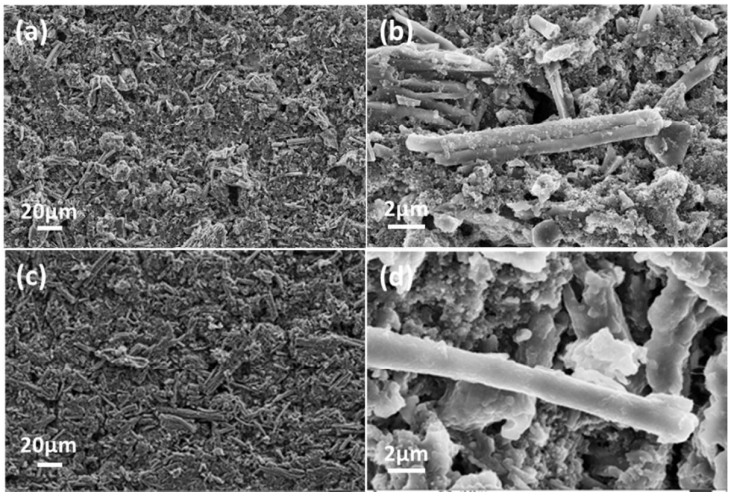

Figure 5

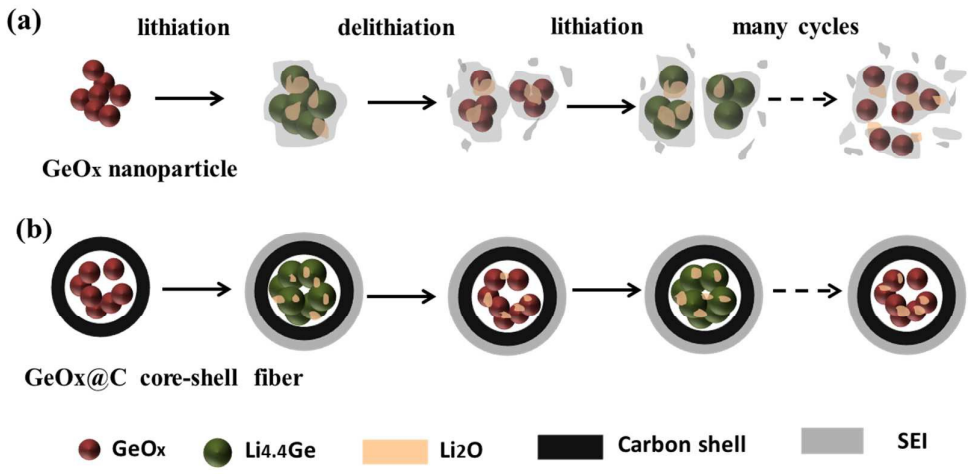

Figure 6

Table of Contents

We demonstrate a facile fabrication that encapsulation GeO_x nanoparticles into hollow carbon shell through co-axial electrospinning. This resultant GeO_x@C core-shell fiber electrode exhibits excellent lithium storage performance, with stable reversible capacity and excellent rate capability.